# Supplementary Information

## Submicron particles of Cr-substituted strontium hexaferrite: anomalous X-ray diffraction studies, hard magnetic properties, millimeter-wave absorption, and research prospects

Evgeny A. Gorbachev, Vasily A. Lebedev, Ekaterina S. Kozlyakova, Liudmila N. Alyabyeva, Antonio Cervellino, Ilya V. Roslyakov, Iana S. Soboleva, Alexey V. Sobolev, and Lev A. Trusov

## §1. Experimental characterization of the samples

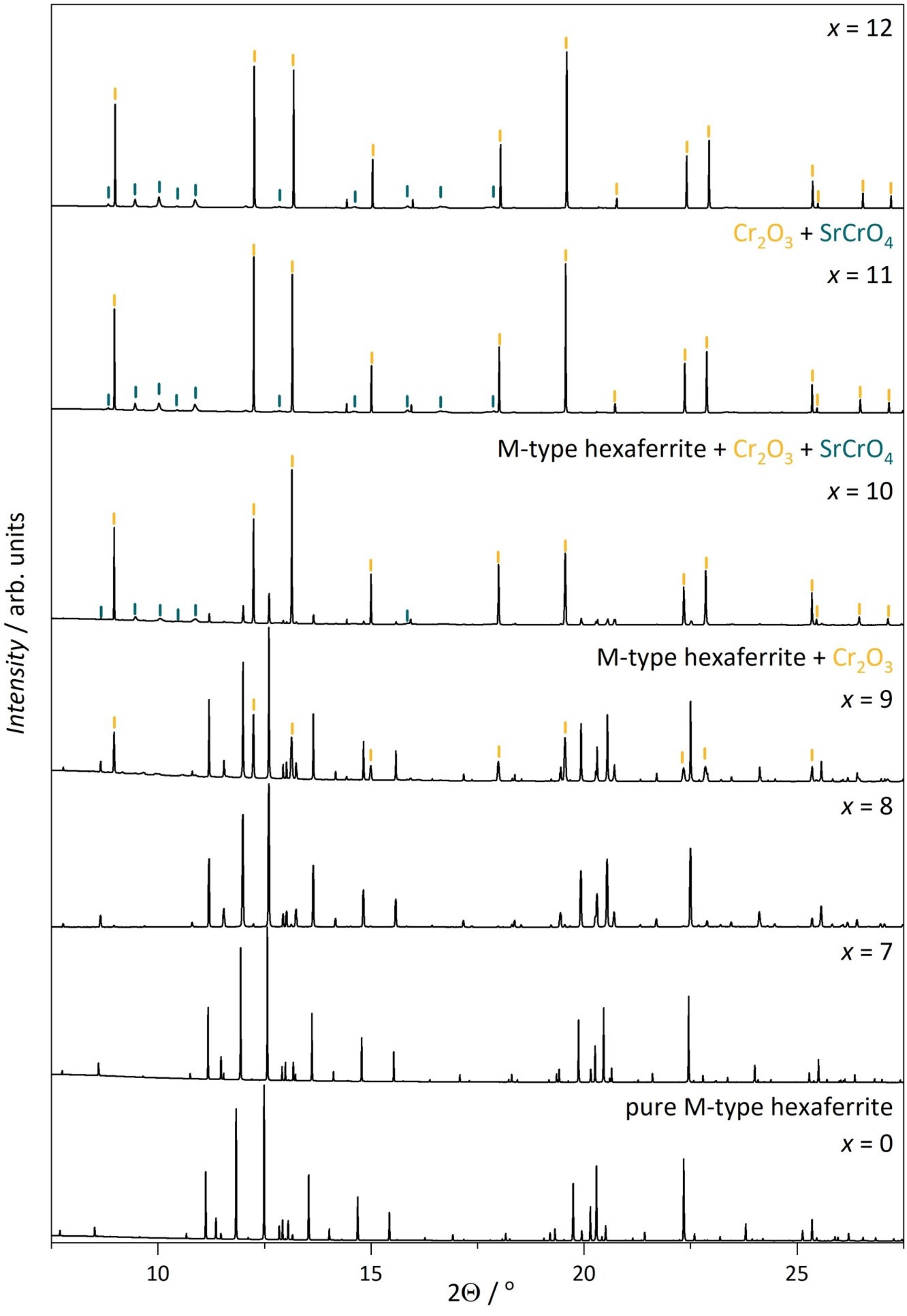

**Fig. S1** Synchrotron powder XRD patterns ($\lambda$ = 0.5690 Å, "neutral" wavelength) and phase analysis of the samples with the nominal chemical composition of $SrFe_{12-x}Cr_xO_{19}$.

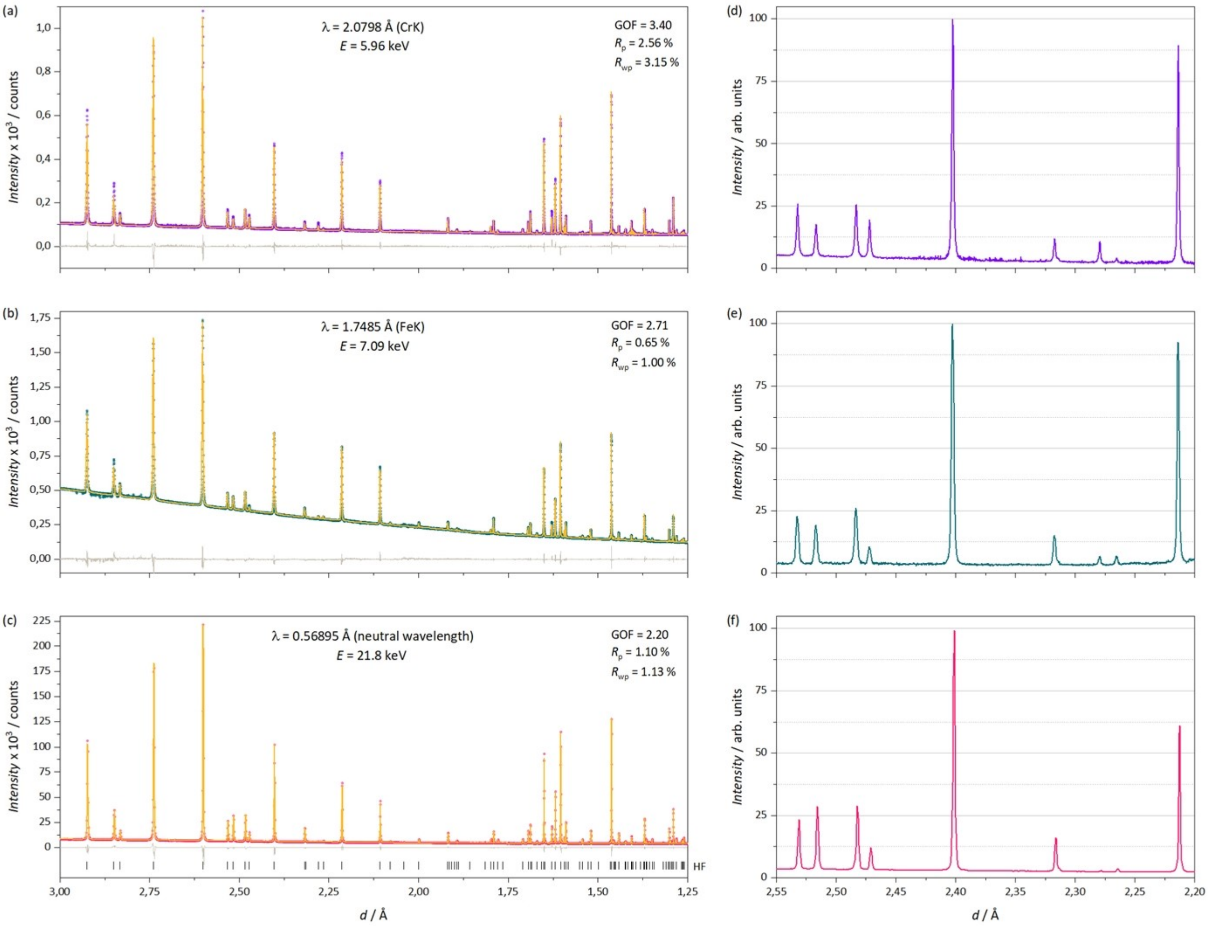

**Fig. S2** The synchrotron anomalous X-ray diffraction patterns of the sample $SrFe_{12-x}Cr_xO_{19}$ ($x$ = 5.5) recorded at three wavelengths and the results of the Rietveld refinement (a – c): the purple, green, and pink plots – experimental data; the yellow lines – theoretical pattern; the grey lines – difference. (d – f) The fine comparison of the XRD patterns collected at CrK, FeK edges, and neutral wavelength.

**Table S1** The parameters of the Rietveld refinement procedure demonstrate a good fit for the X-ray diffraction patterns of the $SrFe_{12-x}Cr_xO_{19}$ samples recorded at different wavelengths, considering 0.56895 Å as the neutral wavelength, while 1.7485 Å and 2.0798 Å correspond to the CrK and FeK absorption edges, respectively. The corresponding mass fraction values of the impurities in the samples were determined from the fits of the spectra recorded at the neutral wavelength.

| Sample (*x*) | 0.56895 Å | | | 1.7485 Å | | | 2.0798 Å | | |
|---|---|---|---|---|---|---|---|---|---|
| | GOF | $R_p$, % | $R_{wp}$, % | GOF | $R_p$, % | $R_{wp}$, % | GOF | $R_p$, % | $R_{wp}$, % |
| 0 | 5.58 | 2.30 | 2.72 | 3.51 | 1.82 | 2.91 | 5.55 | 4.24 | 5.32 |
| 1 | 4.37 | 1.78 | 2.08 | 5.88 | 1.35 | 2.27 | 4.01 | 3.36 | 3.95 |
| 2 | 3.73 | 1.53 | 1.82 | 4.99 | 1.10 | 1.90 | 3.60 | 3.07 | 3.48 |
| 3 | 2.95 | 1.44 | 1.49 | 3.44 | 0.90 | 1.34 | 3.17 | 2.92 | 3.05 |
| 4 | 2.83 | 1.22 | 1.35 | 3.90 | 1.21 | 1.65 | 3.41 | 3.20 | 3.36 |
| 5 | 3.08 | 0.97 | 1.66 | 5.60 | 1.94 | 2.23 | 3.14 | 2.90 | 3.03 |
| 5.5 | 2.20 | 1.10 | 1.13 | 2.71 | 0.65 | 1.00 | 3.40 | 2.56 | 3.15 |
| 6 | 2.60 | 1.18 | 1.27 | 3.06 | 0.73 | 1.19 | 3.46 | 2.46 | 3.13 |
| 7 | 2.74 | 1.19 | 1.30 | 4.55 | 1.24 | 1.92 | 3.23 | 2.56 | 3.02 |
| 8 | 2.46 | 0.95 | 1.23 | 4.52 | 1.35 | 1.96 | 3.32 | 2.52 | 3.02 |

| Sample (*x*) | Overall | | | *Mass fraction*, % | | *Density*, g cm$^{-3}$ |
|---|---|---|---|---|---|---|
| | GOF | $R_p$, % | $R_{wp}$, % | $Cr_2O_3$ | $Fe_2O_3$ | |
| 0 | 5.00 | 2.28 | 3.21 | – | 0.138(1) | 5.104(2) |
| 1 | 4.93 | 1.75 | 2.36 | – | 0.6(1) | 5.100(8) |
| 2 | 4.24 | 1.5 | 2.03 | – | 0.1(5) | 5.10(3) |
| 3 | 3.21 | 1.4 | 1.57 | – | 0.4(4) | 5.10(2) |
| 4 | 3.44 | 1.23 | 1.74 | – | 0.5(3) | 5.10(2) |
| 5 | 4.26 | 1.11 | 2.16 | – | 0.2(7) | 5.10(3) |
| 5.5 | 2.76 | 1.06 | 1.29 | – | – | 5.11(3) |
| 6 | 3.01 | 1.14 | 1.43 | 0.6(5) | – | 5.11(2) |
| 7 | 3.69 | 1.2 | 1.83 | 0.9(6) | – | 5.11(3) |
| 8 | 3.64 | 1.00 | 1.84 | 1.8(6) | – | 5.12(3) |

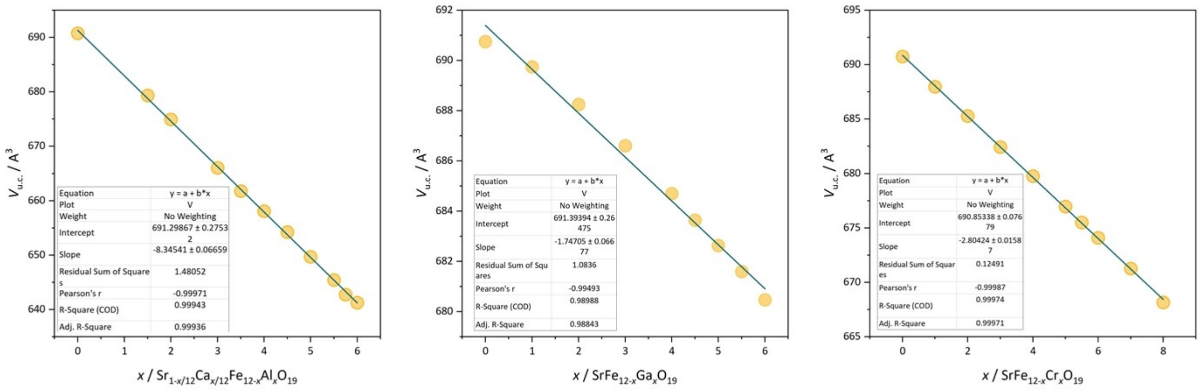

**Fig. S3** Dependencies of the unit cell volume, $V_{u.c.}$, vs. substitution degree in the hexaferrites, and their linear approximation.

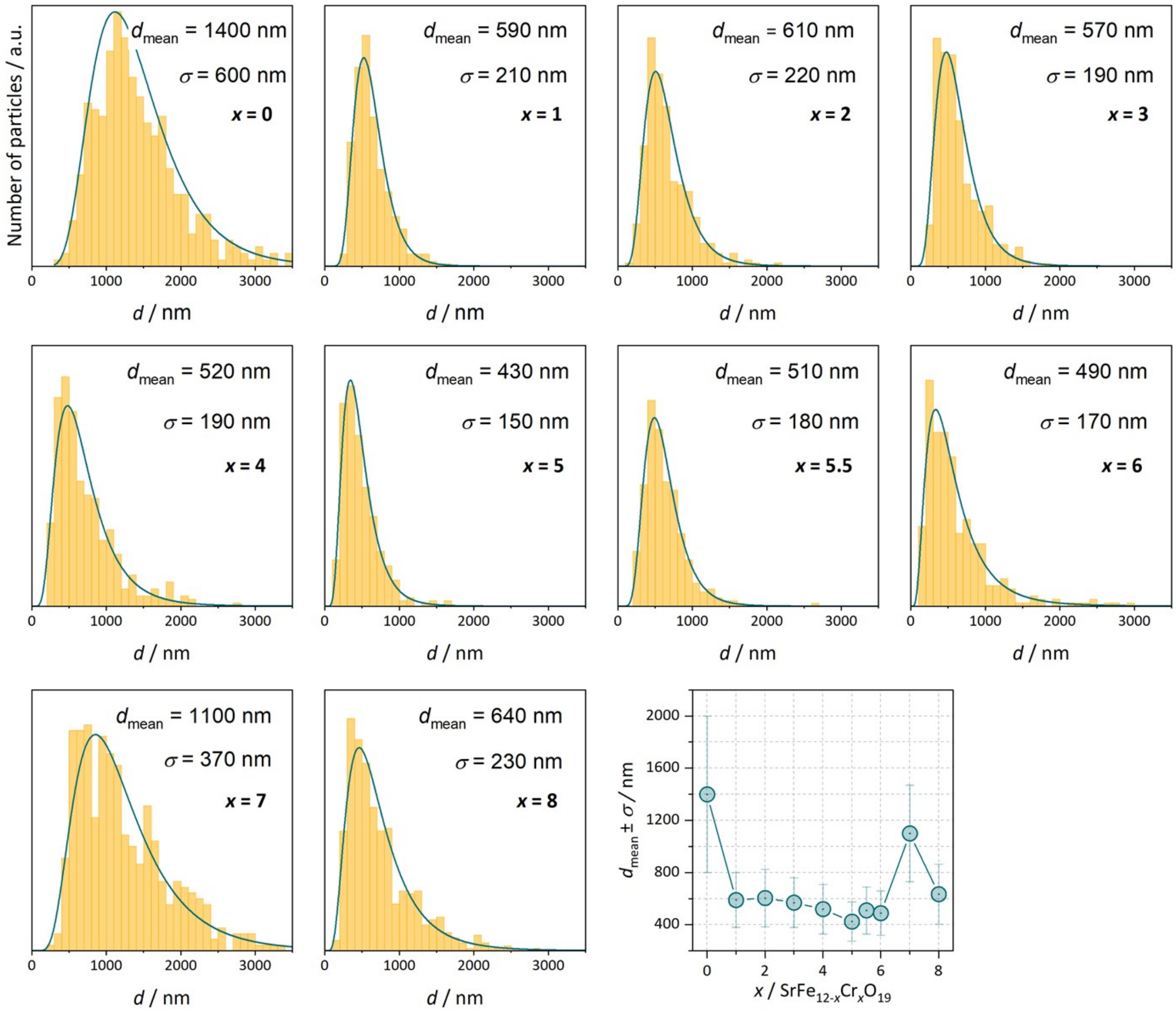

**Fig. S4** SEM histograms of the hexaferrite samples $SrFe_{12-x}Cr_xO_{19}$ fitted with lognormal distribution function. The mean particle size ($d_{mean}$) and standard deviation ($\sigma$) as a function of *x*, derived by fitting SEM histograms with the lognormal distribution.

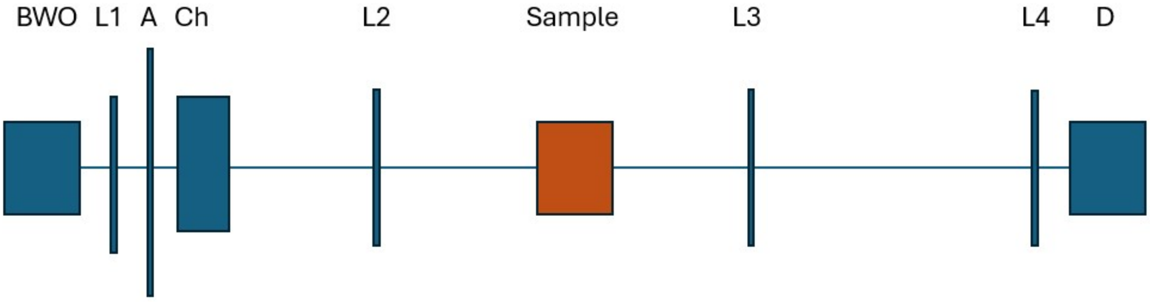

**Fig. S5** The quasi-optic setup for transmission measurements operates in a simple 'transmission geometry' and is shown. It consists of a radiation generator (a backward wave oscillator, BWO) operating in frequency-scanning mode, a set of metallic grid attenuators, a chopper, two pairs of polyethylene lenses, and a Golay cell detector. The frequency scan is achieved by varying the supply voltage of the BWO in small increments. The transmission measurement is conducted in two stages: first, a reference signal is recorded in an open channel, followed by a measurement with the sample placed in the optical path. The detector transmits frequency-dependent intensity data, $I_r$ (reference) and $I_s$ (sample), to the PC. The transmission is then calculated as $T(f)=I_s/I_r$.

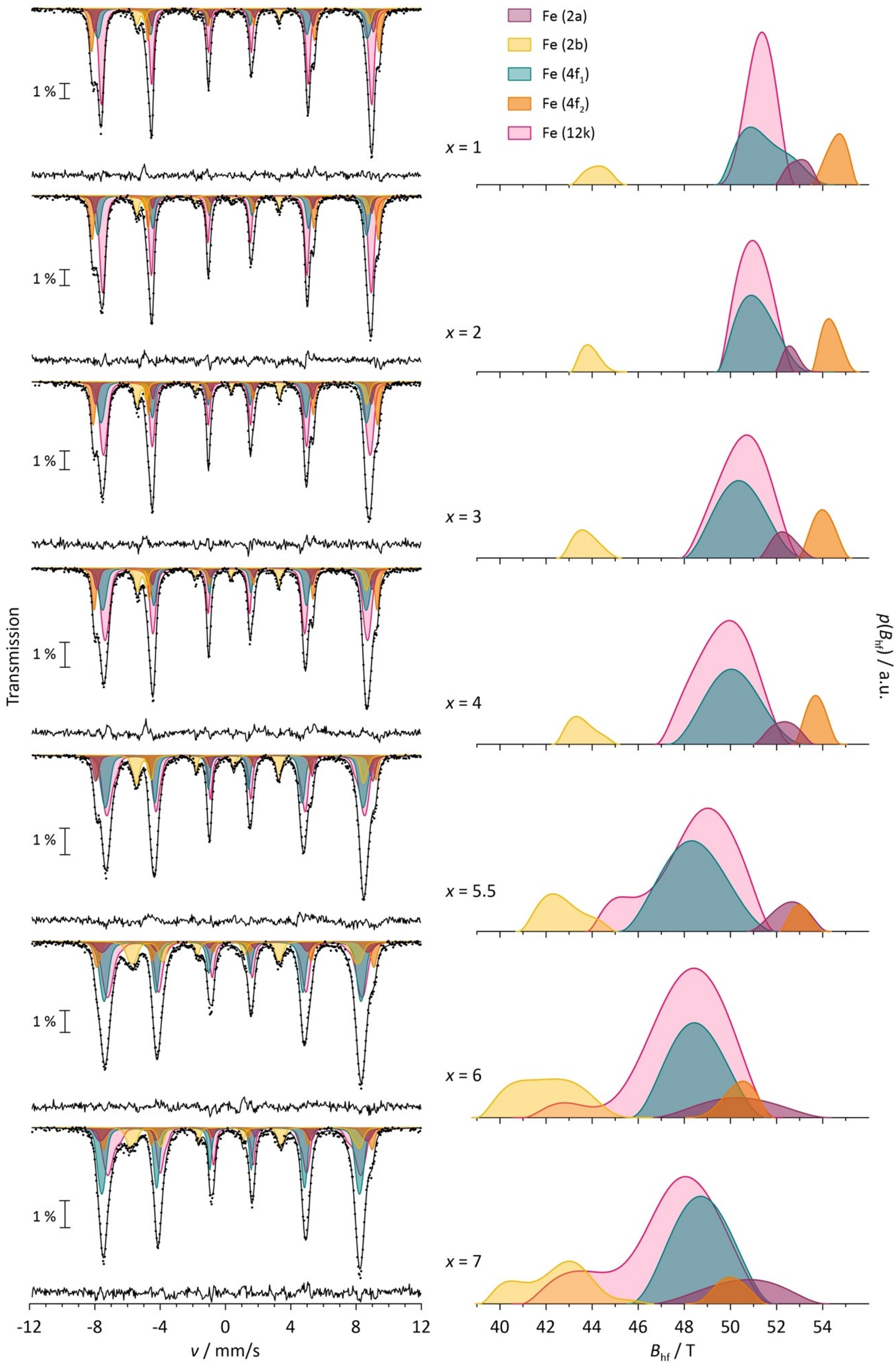

**Fig. S6** (left panel) $^{57}$Fe Mossbauer spectra of SrFe$_{12-x}$Cr$_x$O$_{12}$ hexaferrites recorded at 10 K fitted as superposition of five distributions of the hyperfine magnetic fields (see text); (right panel) The hyperfine magnetic fields distributions.

**Table S2** Hyperfine parameters of the $^{57}$Fe Mössbauer spectra of $SrFe_{12-x}Cr_xO_{19}$ samples measured at $T << T_C$.

| $x$ | Site | $\delta$ / mm/s | $\varepsilon$ / mm/s | $B_{hf}$ / $T$ | $A$ / % |
|---|---|---|---|---|---|
| 1 | 2a | 0.48(1)$^{*}$ | 0.05(1) | 53.0(1) | 10(1) |
| | 2b | 0.44(1) | 1.26(1) | 44.2(1) | 7(1) |
| | $4f_1$ | 0.32(1) | 0.11(1) | 51.4(1) | 19(1) |
| | $4f_2$ | 0.48(1)$^{*}$ | 0.13(1) | 54.6(1) | 18(1) |
| | 12k | 0.48(1)$^{*}$ | 0.20(1) | 51.3(1) | 46(1) |
| 2 | 2a | 0.47(1)$^{*}$ | 0.01(1) | 52.6(1) | 7(1) |
| | 2b | 0.42(1) | 1.21(1) | 43.9(1) | 7(1) |
| | $4f_1$ | 0.36(1) | 0.06(1) | 51.1(1) | 21(1) |
| | $4f_2$ | 0.47(1)$^{*}$ | 0.13(1) | 54.4(1) | 18(1) |
| | 12k | 0.47(1)$^{*}$ | 0.24(1) | 51.0(1) | 48(1) |
| 3 | 2a | 0.47(1)$^{*}$ | 0.02(1) | 52.3(1) | 9(1) |
| | 2b | 0.42(1) | 1.20(1) | 43.7(1) | 9(1) |
| | $4f_1$ | 0.36(1) | 0.14(1) | 50.4(1) | 23(2) |
| | $4f_2$ | 0.47(1)$^{*}$ | 0.14(1) | 54.0(1) | 17(1) |
| | 12k | 0.47(1)$^{*}$ | 0.23(1) | 50.6(1) | 42(1) |
| 4 | 2a | 0.47(1)$^{*}$ | 0.07(1) | 52.3(1) | 9(1) |
| | 2b | 0.42(1) | 1.20(1) | 43.6(1) | 9.2(3) |
| | $4f_1$ | 0.41(2) | 0.13(1) | 50.1(1) | 24(2) |
| | $4f_2$ | 0.47(1)$^{*}$ | 0.14(1) | 53.7(1) | 15(1) |
| | 12k | 0.47(1)$^{*}$ | 0.23(1) | 49.7(1) | 43(2) |
| 5.5 | 2a | 0.47(1)$^{*}$ | 0.06(1) | 52.2(1) | 10(1) |
| | 2b | 0.43(1) | 1.07(1) | 42.7(1) | 13(1) |
| | $4f_1$ | 0.36(1) | 0.18(2) | 48.4(1) | 30(2) |
| | $4f_2$ | 0.47(1)$_{*}$ | 0.20(1) | 53.0(1) | 8(1) |
| | 12k | 0.47(1)$_{*}$ | 0.16(1) | 48.7(1) | 39(3) |
| 6 | 2a | 0.49(1)$_{*}$ | 0.09(1) | 50.4(1) | 7(1) |
| | 2b | 0.45(1) | 0.73(1) | 42.0(1) | 13.9(3) |
| | $4f_1$ | 0.34(1) | 0.10(1) | 48.5(1) | 31(1) |
| | $4f_2$ | 0.49(4)$^{*}$ | 0.11(2) | 50.4(1) | 11(1) |
| | 12k | 0.49(4)$^{*}$ | 0.08(1) | 48.0(1) | 37(1) |
| 7 | 2a | 0.47(1)$^{*}$ | 0.01(1) | 50.6(1) | 9(1) |
| | 2b | 0.41(1) | 0.73(1) | 42.4(1) | 13(1) |
| | $4f_1$ | 0.31(1) | 0.08(1) | 48.7(1) | 36(1) |
| | $4f_2$ | 0.47(1)$^{*}$ | 0.20(2) | 50.0(1) | 9(1) |
| | 12k | 0.47(1)$^{*}$ | 0.03(2) | 47.3(1) | 35(1) |

$\delta$ is an isomer shift, $\varepsilon$ is a quadrupole shift, $B_{hf}$ is a magnetic hyperfine field and $A$ is a relative intensity.

$^{*}$ corresponding values were taken equal to each other.

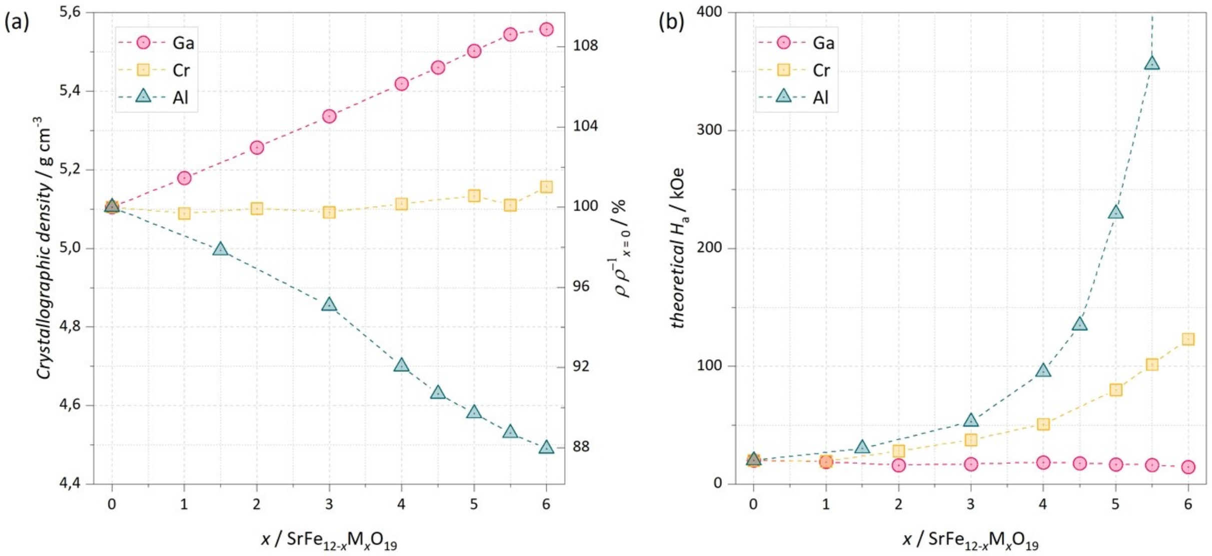

**Fig. S7** (a) Crystallographic density $\rho$ as function of $x$, obtained for the hexaferrite compounds via the Rietveld refinement. (b) The $H_a$ values calculated based on the occupancies data of iron sites using model of additive contributions of iron sublattices in magentocrystalline anisotropy constant $K_1$ and saturation magnetization $M_S$, where a dopant is considered to be diamagnetic, as following:
$M_S(x) = (70/8)\cdot(2/100)\cdot[(100-\alpha_{2a}(x)) + (100-\alpha_{2b}(x)) + 6\,(100-\alpha_{12k}(x)) - 2(100-\alpha_{4f1}(x)) - 2(100-\alpha_{4f2}(x))]$ emu g$^{-1}$,
$K_1(x) = 3.6 - \varepsilon(2/100)\cdot[0.23\alpha_{2a}(x) + 1.4\alpha_{2b}(x) - 6\cdot0.18\alpha_{12k}(x) + 2\cdot0.18\alpha_{4f1}(x) + 2\cdot0.51\alpha_{4f2}(x)]$ erg cm$^{-3}$,
where $\alpha_i$ – a corresponding iron site occupancy factor by a dopant in %, 0.23, 1.4, -0.18, 0.18, and 0.51 cm$^{-1}$/ion are anisotropy constant coefficients according to [1], $\varepsilon = 3.6 / 1.93$ erg cm$^{-2}$ – a normalized coefficient if $K_1$ is considered to be caused only by single-ion anisotropy. An anisotropy field calculated as: $H_a = 2K_1\rho^{-1}M_S^{-1}$. The values of Ga- and Al-series were calculated using the initial data taken from our previous works.[2–4]

## §2. Modeling spin current

**Figure S8** illustrates ferromagnetic resonance precession with labels of vectors, which are used in the Landau-Lifshits equation to calculate the magnetic susceptibility spectra $\chi(f)$ and in the equations of the "Spin current" section to calculate the DC spin currents.

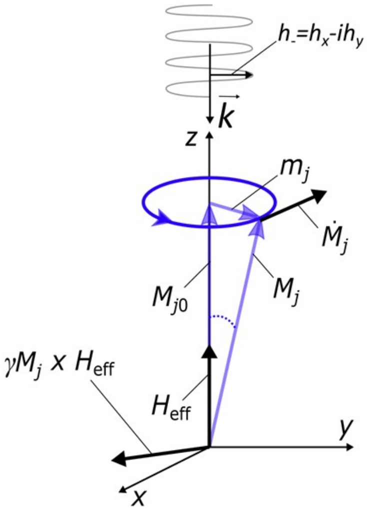

**Fig. S8** Precession of magnetization in a ferromagnet and a falling circular polarized EM wave with an oscillating vector *h*, which can be absorbed by the right-handed precession of the magnetization (FMR mode).

By definition the spin current can be expressed as[5]:

$$J_s = (\hbar/4\pi) g_r^{\uparrow\downarrow} M \times \dot{M},$$

where $g_r^{\uparrow\downarrow}$ denotes the spin-mixing conductance.

The $M \times \dot{M}$ vector product can be expressed by parameterizing as:

$$M = \begin{cases} m_i cos(ft) \\ \pm m_i sin(ft) \\ M_{i0} \end{cases}$$

Taking into account the precession of the magnetic moment around the *z*-axis, we can conclude that the currents in the plane perpendicular to this axis will average out over time, effectively compensating each other. Therefore, to accurately assess the spin current, it suffices to focus solely on its *z*-component. By solving the Landau-Lifshitz equations for the relevant magnetic systems, we derived the *z*-projection of the direct current (DC) spin current:

$$J_S^{DC} = (\hbar/4\pi) g_r^{\uparrow\downarrow} f_r m_{\pm}^2 = (\hbar/4\pi) g_r^{\uparrow\downarrow} f_r \chi_r''^2 h^2$$

By solving the Landau-Lifshitz equation for the simplest case of a two-sublattice ferrimagnet, under the condition that the anisotropy field is much smaller than the molecular (exchange) field, $H_a \ll H_E$, we obtain the expression for the imaginary part of the magnetic susceptibility:

$$\chi_r'' = \frac{\gamma M_{SV}}{\alpha f_r} = \frac{\gamma M_{SV}}{\Gamma}$$

To calculate the DC spin current $J_S^{DC}$ in units of $(\hbar/4\pi) g_r^{\uparrow\downarrow} h^2$ for the hexaferrite samples, we have taken the measured NFMR frequency, the saturation magnetization at 90 kOe multiplied by the crystallographic density of the compound (obtained from the Rietveld refinement), $M_{SV} = \rho M_S$, $\gamma = 2.8$ GHz kOe$^{-1}$, and the damping factors $\Gamma$ were taken from fitting of the corresponding experimental NFMR spectra of the samples. The corresponding data for the M-type hexaferrites partially substituted with $Ga^{3+}$ and $Al^{3+}$ was taken from our previous experimental works.[2–4]

In the same way, for the antiferromagnetic resonance the following expressions are valid:

$$f_{AFMR\pm} = \gamma[\sqrt{(2H_E + H_a)H_a} \pm H_{app}],$$

where $H_{app}$ is the applied magnetic field.

$$\chi_r'' = \frac{\gamma M_0 H_a}{\alpha(H_E + H_a) f_r} = \frac{\gamma M_0 H_a}{(H_E + H_a)\Gamma}$$

To model $J_S^{DC}$ for the antiferromagnetic resonance in $MnF_2$, we have taken the following parameters: $H_a = 8800$ Oe, $H_E = 556\,000$ Oe, $M_0 = 590$ G at 0 K, and the highest $f_r = 261$ GHz at 4.2 K from[6]; and $\gamma = 0.0028$ GHz Oe$^{-1}$, $\Gamma = 2.61$ GHz. Thus, the $J_S^{DC} \approx 0.025$ units of $(\hbar/4\pi) g_r^{\uparrow\downarrow} h^2$.

## References

1 Y. Xu, G. L. Yang, D. P. Chu and H. R. Zhai, *Physica Status Solidi (B)*, 1990, **157**, 685–693.

2 E. A. Gorbachev, L. A. Trusov, A. E. Sleptsova, E. S. Kozlyakova, L. N. Alyabyeva, S. R. Yegiyan, A. S. Prokhorov, V. A. Lebedev, I. V. Roslyakov, A. V. Vasiliev and P. E. Kazin, *Materials Today*, 2020, **32**, 13–18.

3 L. A. Trusov, E. A. Gorbachev, V. A. Lebedev, A. E. Sleptsova, I. V. Roslyakov, E. S. Kozlyakova, A. V. Vasiliev, R. E. Dinnebier, M. Jansen and P. E. Kazin, *Chemical Communications*, 2018, **54**, 479–482.

4 E. A. Gorbachev, L. A. Trusov, M. Wu, A. V. Vasiliev, R. D. Svetogorov, L. N. Alyabyeva, V. A. Lebedev, A. E. Sleptsova, M. A. Karpov, Y. M. Mozharov, B. P. Gorshunov and P. E. Kazin, *Journal of Materials Chemistry C*, 2021, **9**, 13832–13840.

5 V. Baltz, A. Manchon, M. Tsoi, T. Moriyama, T. Ono and Y. Tserkovnyak, *Reviews of Modern Physics*, 2018, **90**, 015005.

6 F. M. Johnson and A. H. Nethercot, *Physical Review*, 1959, **114**, 705–716.